Crystal structure of microsomal prostaglandin E_2 synthase provides insight into diversity in the MAPEG superfamily

Tove Sjögren[a,1], Johan Nord[b], Margareta Ek[a], Patrik Johansson[a], Gang Liu[b], and Stefan Geschwindner[a,1]

[a]Discovery Sciences, AstraZeneca R&D Mölndal, S-43183 Mölndal, Sweden; and [b]Department of Neuroscience, AstraZeneca R&D Södertälje, S-151 85 Södertälje, Sweden

Edited by R. Michael Garavito, Michigan State University, East Lansing, MI, and accepted by the Editorial Board January 17, 2013 (received for review October 24, 2012)

Prostaglandin E_2 (PGE_2) is a key mediator in inflammatory response. The main source of inducible PGE_2, microsomal PGE_2 synthase-1 (mPGES-1), has emerged as an interesting drug target for treatment of pain. To support inhibitor design, we have determined the crystal structure of human mPGES-1 to 1.2 Å resolution. The structure reveals three well-defined active site cavities within the membrane-spanning region in each monomer interface of the trimeric structure. An important determinant of the active site cavity is a small cytosolic domain inserted between transmembrane helices I and II. This extra domain is not observed in other structures of proteins within the MAPEG (Membrane-Associated Proteins involved in Eicosanoid and Glutathione metabolism) superfamily but is likely to be present also in microsomal GST-1 based on sequence similarity. An unexpected feature of the structure is a 16-Å-deep cone-shaped cavity extending from the cytosolic side into the membrane-spanning region. We suggest a potential role for this cavity in substrate access. Based on the structure of the active site, we propose a catalytic mechanism in which serine 127 plays a key role. We have also determined the structure of mPGES-1 in complex with a glutathione-based analog, providing insight into mPGES-1 flexibility and potential for structure-based drug design.

membrane protein | X-ray crystallography | enzyme mechanism

Prostaglandins are potent lipid messengers and are involved in numerous homeostatic biological functions [for a review of eicosanoid biology, see review by C. D. Funk (1)]. They are enzymatically derived from the essential fatty acid arachidonic acid and the synthesis proceeds via the formation of prostaglandin H_2 (PGH_2), a reaction catalyzed by the constitutively active cyclooxygenase COX-1 and the inducible cyclooxygenase COX-2. PGH_2 acts as a substrate for a range of terminal prostaglandin synthases, including the PGE synthases (PGES, EC 5.3.99.3) that convert PGH_2 to PGE_2.

Microsomal prostaglandin E_2 synthase-1 (mPGES-1), colocalized and up-regulated in concert with COX-2, is the major source of inducible PGE_2 and is associated with inflammation and pain (2). Several studies support a role for mPGES-1 also in cancer cell proliferation and tumor growth (3). Because treatment with COX-2 selective inhibitors is associated with elevated cardiovascular risk, safer approaches involving, for example, PGE_2 reduction, are needed (4). Mice deficient in mPGES-1 have shown significantly reduced effect on hypertension, thrombosis, and myocardial damage compared with inhibition or disruption of COX-2, suggesting mPGES-1 to be a potential target for pharmaceutical intervention in various areas of diseases (2, 5).

mPGES-1 belongs to a superfamily of Membrane-Associated Proteins involved in Eicosanoid and Glutathione metabolism, the MAPEG family (6). Members of the MAPEG family can be found in prokaryotes and eukaryotes but not in archaea (7). The most closely related MAPEG member is the microsomal glutathione transferase-1 (MGST1), which shares 39% sequence identity with mPGES-1. Leukotriene C_4 (LTC_4) synthase, 5-lipoxygenase activating protein (FLAP), MGST2, and MGST3 are more distantly related with a sequence identity of 15–30%. Initial structural characterization of the MAPEG family was done using electron crystallography and showed that the members contain four transmembrane helices and are organized as trimers (8, 9). This was later confirmed by the X-ray crystal structures of FLAP (10) and LTC_4 synthase (11, 12). There are also low-resolution 3D electron crystallography structures of MGST1 and mPGES-1 (13, 14). However, these structures did not allow for detailed structural analysis, and concerns regarding the accuracy of the MGST1 structure have been raised (15).

Here we present the 1.2 Å X-ray structure of human microsomal PGE_2 synthase-1. The structure differs significantly from the previously reported electron crystallography structure of mPGES-1 (14). In particular, glutathione binding and coordination are different in the two structures. Moreover, the structure presented here reveals a small structured domain inserted between helices I and II that contributes to the active site cavity. This domain is not present in LTC_4 synthase (11, 12) or FLAP (10), but is likely to be present in MGST1. Based on the atomic detail as well as mutagenesis data available in the literature, we propose a mechanism for mPGES-1–catalyzed isomerization of PGH_2 to PGE_2. The structure also offers some insight into a possible mechanism for monomer cross-talk, implicated by recent data indicating that mPGES-1 displays 1:3-site reactivity (16). Finally, the structure provides an excellent starting point for rational design of mPGES-1 inhibitors.

Results

Overall Structure. Human mPGES-1 was cloned and overproduced in a baculovirus expression system. The structure of mPGES-1 in complex with glutathione (GSH) was solved using the anomalous dispersion from mercury atoms, incorporated into mPGES-1 crystals by soaking. The asymmetric unit contains a single mPGES-1 molecule with a bound GSH. Similar to the LTC_4 synthase and the FLAP, the mPGES-1 overall fold consist of a four-helix bundle that packs together to form a homotrimer (Fig. 1). The mPGES-1 structure contains a 20-aa insert between

Author contributions: T.S., J.N., M.E., P.J., G.L., and S.G. designed research; T.S., J.N., M.E., P.J., G.L., and S.G. performed research; T.S., J.N., M.E., P.J., G.L., and S.G. analyzed data; and T.S., J.N., M.E., P.J., G.L., and S.G. wrote the paper.

Conflict of interest statement: T.S., J.N., M.E., P.J., G.L., and S.G. were all employees and shareholders of AstraZeneca at the time the work presented here was conducted.

This article is a PNAS Direct Submission. R.G. is a guest editor invited by the Editorial Board.

Data deposition: The sequences have been deposited in the Protein Data Bank, www.pdb.org (PDB ID codes 4AL0 and 4AL1).

[1]To whom correspondence may be addressed. E-mail: tove.sjogren@astrazeneca.com or stefan.geschwindner@astrazeneca.com.

This article contains supporting information online at www.pnas.org/lookup/suppl/doi:10.1073/pnas.1218504110/-/DCSupplemental.

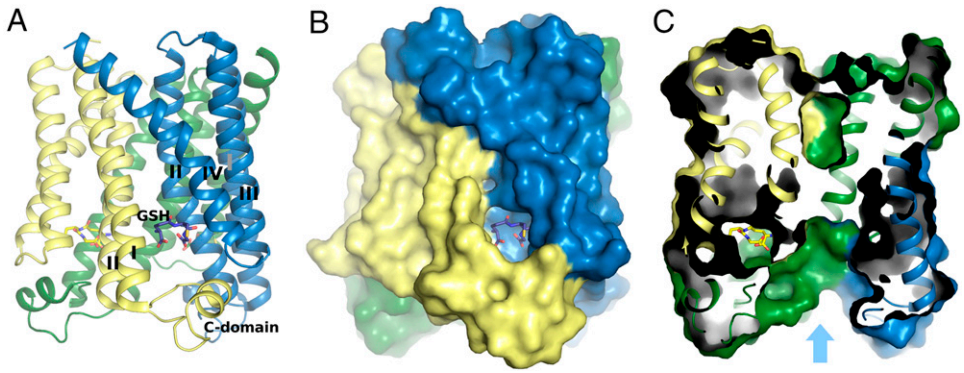

Fig. 1. Overall structure of mPGES-1. (*A*) Structure of the mPGES-1 trimer. The asymmetric unit contains one monomer; the full trimer was generated by applying the crystallographic symmetry. Monomers are shown in blue, yellow, and green, respectively. The bound GSH molecule is shown in stick representation. (*B*) Surface representation of the mPGES trimer using the same orientation as in (*A*). (*C*) Cross-section along the crystallographic three-fold axis showing the central cone-shaped cavity on the cytosolic side of mPGES. The opening of the cavity is indicated with a block arrow.

helices I and II that forms a small positively charged domain consisting of two structured loops and a short helix, henceforth referred to as the C-domain. The positive charge is consistent with the proposed topology of mPGES-1 where the N and C termini are located in the endoplasmic reticulum lumen. The overall helix angles relative to the membrane normal are 24°, 20°, 18°, and 40°, respectively. Helices II and IV contain pronounced kinks caused by the presence of two proline residues (Pro81 and Pro136) that disrupt the helix hydrogen bonding network. The kink in helix II gives rise to a large cytoplasmic cone-shaped cavity in the center of the mPGES-1 trimer (Fig. 1*C*). The length of the cone is about 16 Å and the narrow end is located well within the membrane-spanning region. Each four-helix bundle is stabilized by a cluster of polar residues including Lys26, Asn74, Asp75, Arg110, and Thr114 bridged by two in-membrane water molecules connecting helices I, II, and III.

Active Site. The N-terminal parts of helices II and IV, together with the C-terminal part of helix I and the cytoplasmic domain from an adjacent molecule, form an ∼15-Å-deep cavity with an opening measuring 12 × 9 Å (Fig. 1*B*). The mPGES-1 trimer contains three such cavities in each of the monomer interfaces. Strong F_o-F_c density for a bound glutathione molecule was found in a bent conformation (Fig. 2*A*). The GSH is coordinated by hydrogen bonds involving the side chains of Arg73, Asn74, Glu77, His113, Tyr117, Arg126, and Ser127 from helices II and IV and the side chain of Arg38 from helix I in a symmetry-related molecule (Fig. 2*B*). In addition to the hydrogen bonds, the phenol group of Tyr130 forms a π-stacking interaction with the gamma peptide linkage between the cysteine and the glutamate side chain of GSH. The C-domain does not contribute any direct interactions to the cofactor. However, the side chain of Asp49 is involved in a close salt bridge with Arg126, indirectly contributing to the environment of the glutathione. Asp49 is also highly conserved in the MGST1/mPGES-1 subgroup of MAPEGs (7). Although the glutathione appears to be bound at full occupancy, two of the side chains interacting with the cofactor display double conformations: Arg73 and Ser127. The remaining volume of the GSH-binding cavity constitutes a small pocket. The substrate for mPGES-1, PGH_2, is composed of a more or less spherical head group with two tails, about 10 and 8 Å long in their extended conformations. The spherical head group can be modeled into the pocket with the two flexible tails protruding into the lipid bilayer or the membrane-cytosol interface where a number of interactions with the protein could be anticipated. Based on the size and shape and the apparent scope for favorable interactions with the substrate, we propose this cavity to be the site of catalytic activity.

GSH Analog Complex Structure. To probe the mPGES-1 active site, we solved the structure of mPGES-1 cocrystallized with a GSH analog: 1-(4-phenylphenyl)-2-(S-glutathionyl)-ethanone (bis-phenyl-GSH) to a resolution of 1.95 Å (Fig. 2*C*). From the electron density, it is clear that the glutathione has not been completely replaced by the analog during cocrystallization; the occupancy is ∼0.7 for the analog and 0.3 for the GSH as assessed from B factors of the bis-phenyl substituent of the analog and the thiol of glutathione. The tripeptide moiety of the analog mostly overlaps

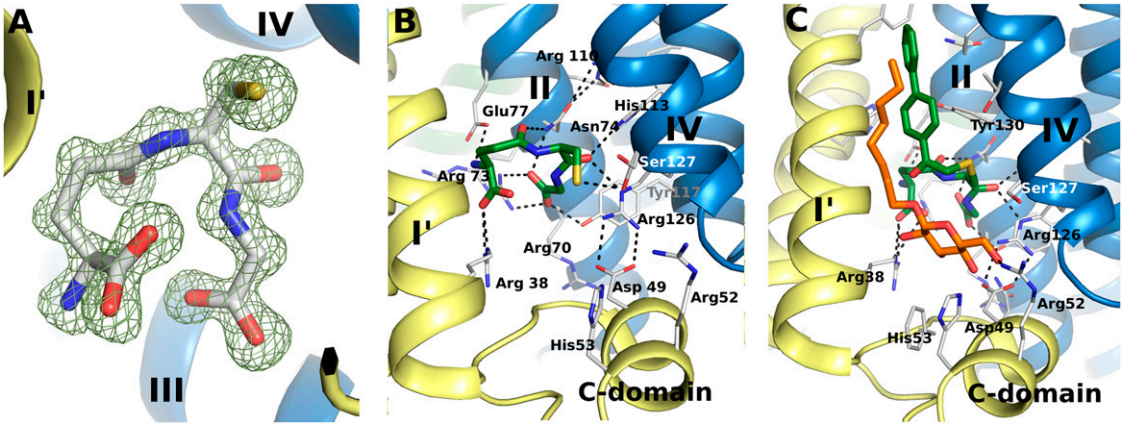

Fig. 2. Structure of the active site in mPGES-1 at the monomer interface. (*A*) F_o-F_c electron density map for the GSH contoured at 4σ. (*B*) Interactions between mPGES-1 and GSH. The Arg38 side chain originates from the symmetry-related monomer. (*C*) mPGES-1 in complex with bis-phenyl-GSH. Bis-phenyl-GSH is shown in green stick representation. A β-octyl glucoside (orange stick representation) is bound to the active site. Distances between β-octyl glucoside and mPGES-1 shorter than 3.2 Å are indicated with dashed lines. This figure is provided as a stereo diagram in Fig. S1.

well with glutathione, the exception being a 0.5-Å shift centered around the carbonyl group of the γ peptide bond. The bis-phenyl substituent is oriented toward the center of the membrane in the shallow groove between helices I and IV from adjacent monomers. Although the substituent is bulky, binding has very small effects on the overall structure of mPGES-1; the only significant difference is a slight shift in the position of the side chain of Tyr130. The shift in Tyr130 is likely linked to the observed shift in the glutathione backbone of the inhibitor. Interestingly, the complex structure also features a bound β-octyl glucoside molecule with the aliphatic chain stacked against the hydrophobic bis-phenyl group and the glucoside moiety involved in several hydrogen bonding interactions in the putative substrate-binding cavity.

Discussion

The high resolution X-ray crystallography structure of mPGES-1 presented here reveals unprecedented molecular detail of this integral membrane enzyme. Key findings include unambiguous identification of the cofactor glutathione-binding mode and localization of a putative active site.

The mPGES-1 structure also illustrates the structural diversity within the MAPEG family. X-ray structures for two other MAPEG family members [LTC_4 synthase (11, 12) and FLAP (10)]have been published. Although LTC_4 synthase and FLAP are closely related with a sequence homology of more than 40% within the membrane-spanning domain, mPGES is more distantly related, displaying sequence homology of around 15% to FLAP and LTC_4 synthase (Fig. S2). Despite the distant relationship, the structures can be superimposed on mPGES-1 with rmsd of 1.8 and 1.9 Å, respectively, for Cα atoms in the transmembrane region. The most prominent differentiating feature of the mPGES-1 structure is the insert between TMI and TMII that folds into a small well-structured domain (the C-domain) that forms part of the active site cavity. Based on sequence homology, the C-domain is likely to be conserved also in the MGST1 (Fig. S2) and demonstrates diversity of topology within the MAPEG superfamily. Low-resolution electron crystallography data on MGST1 support this hypothesis, although the quality of the data did not permit modeling (13).

An unexpected observation in the mPGES-1 structure is the large cone-shaped cavity extending from the cytosolic side along the symmetry axis of the trimer with the top of the cone in close contact with the three active site cavities. The side chain of Arg73 blocks the connection between the central cavity and the active site. However, this residue has two discrete conformations. In the first conformation, Arg73 coordinates one of the glutathione carboxylate groups resulting in a separation of the cavities (Fig. 3 *A* and *C*). In the alternative orientation, it is making an interaction with the main chain carbonyl of Leu69 of an adjacent molecule and the solvent structure in the central cavity. The nearby side chain of Glu77 makes an interaction with Arg73 in both conformations, although via different atoms. In the second conformation, the active site pocket and the central cavity form a continuous surface (Fig. 3 *B* and *C*). The significance of this interconnected super pocket is unclear. It could provide an explanation for the mechanism by which the highly soluble GSH enters the active site located within the hydrophobic bilayer of the endoplasmic reticulum membrane. The connection between the cytosol and the active site could also have a role in solvent exchange between the water bulk and the catalytic cavity. Given the geometric arrangement of the three active sites and the GSH coordination via Arg73, an element of cooperativity could also be anticipated. Interestingly, such a mechanism has been suggested based on biochemical data both for MGST1 (17) and, more recently, for mPGES-1 (16). However, Arg73 is only conserved in mPGES-1 from higher vertebrates, implicating that any mechanism relating to Arg73 conformation might not translate to other MAPEG family members.

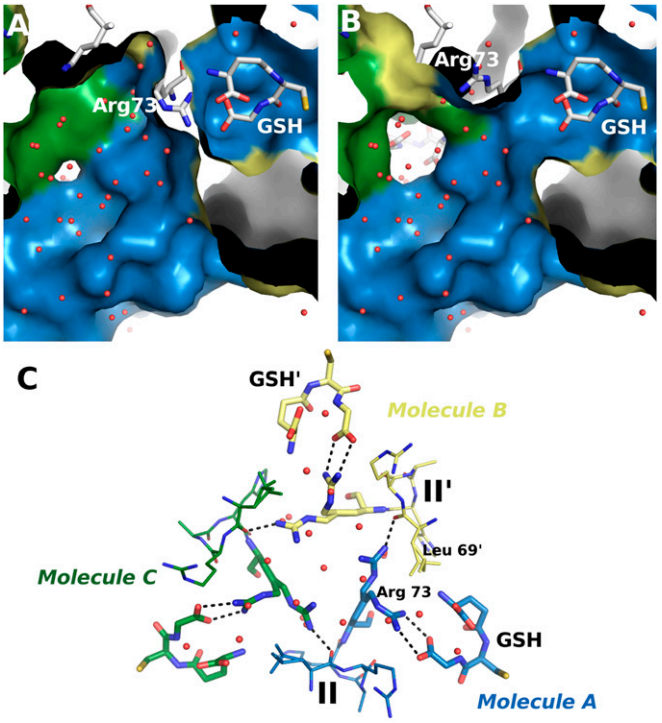

Fig. 3. Connectivity between the central cavity and active site in mPGES-1. (*A*) Surface representation of the active site and the central cavity showing Arg73 in the GSH coordinating conformation. (*B*) Same as (*A*) but with Arg73 in the monomer interaction conformation. (*C*) View of both Arg73 conformations from the luminal side highlighting the potential for cross-talk between the monomers. GSH and a short stretch of helix II is shown for each monomer in blue, yellow, and green, respectively.

The proline-induced kink in helix II, giving rise to the cone-shaped cavity on the cytosolic side of mPGES, is a common feature in the MAPEG structures determined to date. However, the position of the mPGES-1 proline is shifted one step compared with the LTC_4 synthase and the FLAP structures, resulting in dramatic differences in the shape of the central cavities (Fig. 4). In FLAP, there is a large cavity on its luminal side, also pointed out by Ferguson et al. (10). In LTC_4 synthase (11, 12), the central cavity is more hourglass shaped with smaller but significant cavities on both sides of the membrane.

Despite the low sequence homology between mPGES-1 and LTC_4 synthase, the glutathione-binding site is well conserved. In both cases, glutathione binds in a horseshoe conformation and five of the eight interactions observed in mPGES-1 are conserved in LTC_4 synthase (Fig. 5 *A* and *B*). However, Arg70 corresponding to the highly conserved Arg51 in LTC_4 synthase does not interact with the GSH in mPGES-1. This role is instead taken over by one of the conformations of Arg73 (see the previous paragraph). Although there are similarities in GSH coordination, the shape of the pocket around the cofactor is very different. LTC_4 synthase is not only lacking the structured C-domain, but also displays a different lining of the crevice making the remaining pocket more restricted around the thiol (Fig. 5 *C* and *D*). Instead, substrate binding in LTC_4 synthase is suggested to imply an extended cavity on the opposite side of GSH, lined by helix I and IV from two adjacent monomers (11, 12). A similar cavity in FLAP has been identified as an inhibitor binding site (10). This proposed binding site has no counterpart in mPGES-1 because of the side chain of Tyr130 that stacks on top of GSH, making the crevice along the trimer interface very shallow. The differences in glutathione coordination and overall structure are

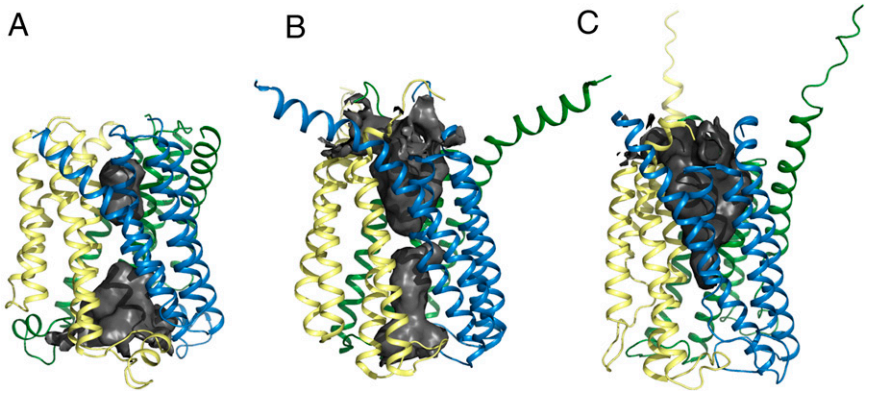

Fig. 4. Central cavities in MAPEG family members. (*A*) mPGES-1, (*B*) LTC4S [Protein Data Bank (PDB) ID code 2UUH (12), and (*C*) FLAP [PDB ID code 2Q7M (10)]. Cavities centered on the threefold access are shown as gray surfaces.

likely reflecting the different functions of these two enzymes: mPGES-1 catalyses isomerization of PGH_2, using glutathione as a cofactor whereas in LTC_4 synthase glutathione is a cosubstrate that is conjugated to the substrate LTB_4 to form LTC_4.

The detailed geometry of the active site leads to insights into the catalytic mechanism of mPGES-1. The presented structural information, together with existing mutagenesis data, guides the assignment of specific functions to amino acid residues during enzyme catalysis and helps to highlight some further distinctions from LTC_4 synthase. In LTC_4 synthase, the glutathione thiol group is coordinated by a highly conserved arginine side chain, Arg104 (11, 12). This residue was recently suggested to be the primary residue responsible for promoting and stabilizing the glutathione thiolate in all catalytically active MAPEG family members (18). However, the corresponding Arg126 in mPGES-1 is unlikely to play a similar role in the activation of the glutathione thiol because it is part of a strong bidentate complex with Asp49 (Fig. 2*B*). This is further supported by earlier observations that the mutation of Arg126 to either Ala or Glu shifts the enzyme activity toward a reductase activity that, similar to the PGE_2 isomerization reaction, requires a glutathione thiolate to initiate the catalytic cycle (19). Instead, the structural data strongly suggest that formation and stabilization of the glutathione thiolate is promoted by the hydroxyl group of Ser127 (Figs. 2 and 6). This is a common theme in, for example, soluble glutathione S-transferases, where a hydroxyl group of a tyrosine or serine

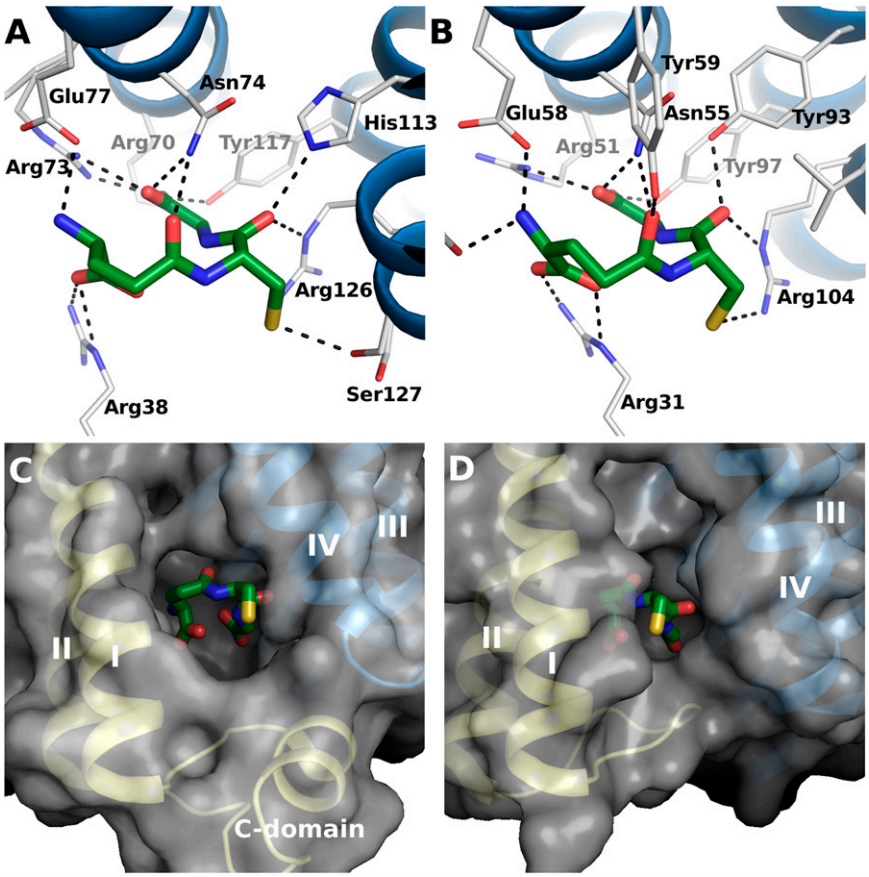

Fig. 5. Comparison of mPGES and LTC_4 synthase. View of the glutathione coordination in mPGES-1 (*A*) and LTC_4 synthase (*B*). Potential hydrogen bonds are denoted with black dashed lines. (*C* and *D*) Surface representations of mPGES-1 and LTC_4 synthase highlighting the differences in the shape of the active site cavities.

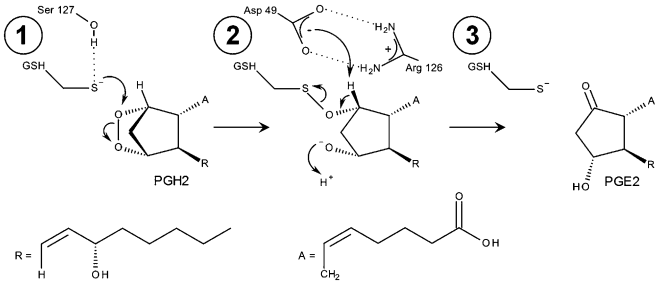

Fig. 6. Suggested mechanism of PGH_2 isomerization to PGE_2 by mPGES-1. (*1*) Ser127 activates the thiol of GSH to form a thiolate anion that exerts a nucleophilic attack on the endoperoxide oxygen atom at the C-9 carbon of PGH_2 to produce an unstable reaction intermediate. (*2*) The subsequent proton abstraction at C-9 followed by S·O bond cleavage is mediated by Asp49 that forms a bidentate complex with Arg126. (*3*) This results in the regeneration of the reactive thiolate anion and the formation of the product PGE_2.

residue makes a corresponding hydrogen bond, which is expected to decrease the pK_a of the thiol group, resulting in a deprotonation at neutral pH (20).

Because the stabilized glutathione thiolate can act either as a base or as a nucleophile, two different mechanistic pathways can be envisaged for the enzymatic catalysis. One pathway could comprise a deprotonation at the C-9 carbon in conjunction with the cleavage of the peroxide bond. An alternative mechanism that is frequently proposed for this step of the enzymatic reaction (21) involves a nucleophilic attack of the thiolate anion at one of the peroxide oxygen atoms to form a mixed sulfide, followed by deprotonation and S·O bond cleavage (Fig. 6). Both scenarios require the presence of another residue to function as a base to facilitate either the regeneration of the thiolate or to enable proton transfer from the C-9 carbon. Arg126 and Asp49 are in close proximity to the putative reaction center, and as ionizable amino acid residues they could fulfill this role. Even though arginine residues are generally considered poor candidates for the role of general bases, there is evidence that they can facilitate general base catalysis (22). However, it is unlikely that this residue is deprotonated in mPGES-1, because the bidentate interaction with Asp49 is expected to increase the pK_a value of Arg126. Furthermore, mutagenesis data indicate that the mutation of Arg126 impairs, but does not abolish, the formation of PGE_2 (19). Taken together, these data suggest that Asp49 is the residue acting as a base during proton abstraction. This mechanism appears plausible because only a minor rearrangement of the mixed sulfide of glutathione and PGH_2 is required to bring Asp49 in close proximity to facilitate proton transfer. The primary role of Arg126 is likely the alteration of the Asp49 pK_a to increase the effectiveness of this reaction and to prevent reduction of the reaction intermediate. This is supported by Arg126 mutagenesis studies (19), which indicate that the mixed sulfide intermediate can indeed be reduced to $PGF_{2\alpha}$ by the R126Q mutated enzyme, a product that is only distinguished from PGE_2 through a reduction of the ketone at C-9 to a secondary alcohol. The presented structure together with the enzymatic data on the Arg126-deficient mutants would allow drawing of a plausible scenario, where in absence of Arg126, the partially deprotonated Asp49 acts as a proton donor. This will promote $PGF_{2\alpha}$ formation, which is unlikely when forming a bidentate complex with Arg126, as seen in the wild-type enzyme. However, further mutagenesis studies involving Asp49 and also Ser127 will be required to complete and support the outlined reaction mechanism.

Membrane proteins are often flexible, and flexibility is part of the function in, for example, G protein–coupled receptor (23) or transport across membranes (24). mPGES-1 in contrast appears to be very rigid, stabilized by several interhelix hydrogen bonds within the membrane spanning region. Moreover, cocrystallization with a glutathione analog with a bulky bis-phenyl substituent on the thiol group failed to induce any differences in the overall structure. However, the previously published mPGES-1 electron crystallography structure to 3.5 Å resolution (14) deviates significantly from the high-resolution structure with an rmsd for all 142 Cα atoms of 4.7 Å. In the low-resolution structure, there is no access to the active site from the membrane; the authors propose that it represents a closed conformation. The low-resolution structure lacks the kink in helix IV and although the C-domain could not be fully modeled in the low-resolution structure, there is little overlap between the modeled parts. Moreover the glutathione is modeled in a different orientation ~3 Å from the binding site seen in the high-resolution structure. Although these differences along with low completeness of the electron crystallography data (<60%) and high R factors (>35%) of the final model suggest there may be problems with the low-resolution structure, it cannot be entirely excluded that mPGES-1 may exist in different conformations. It would be interesting to see the electron crystallography data reinterpreted in light of the new structure.

The structure presented here provides a good starting point for rational design of mPGES-1 inhibitors. In the bis-phenyl-GSH complex structure, a β-octyl glucoside molecule is bound in the active site pocket and hydroxyl groups of the head moiety are involved in several hydrogen bonds (Fig. 2*C*), illustrating the scope for exploring polar interaction in this area. Inhibitor binding to the active site is supported by recent hydrogen/deuterium exchange kinetics experiments, indicating changes in exchange rates in the mPGES-1 peptide consisting of residues 37–54 upon binding of potent inhibitors (25). Because the active site is very shallow, orthosteric inhibition is likely to imply residues outside the catalytic cavity also. The possibility of allosteric inhibition cannot be excluded. However, the stability of the protein, implied by the interhelical hydrogen bond cluster and the lack of observation of flexibility upon ligand binding makes it unlikely that highly potent allosteric inhibitors can be developed.

The putative inhibitor binding site is not completely conserved across species and there are reports of compounds displaying good in vitro potency in human mPGES-1 but little or no effect in rat (26, 27). Based on the low-resolution electron crystallography structure (14) and the assumption that the active site would be analogous to LTC_4 synthase, a series of point mutations were made to rationalize the lack of species cross-over (27). A combination of Thr131, Leu135, and Ala138 mutations were shown to have an effect on altering species selectivity, although the effect did not account for the full difference in inhibition. Based on the structure presented here, Arg52 and His53 are additional likely culprits for the species differences. However, because of a lack of structural data, these were overlooked in the mutational studies. Both of these side chains are located on the C-domain, potentially impacting on ligands interfering with the PGH_2 head group binding (Fig. 2).

The high-resolution mPGES-1 structure explains some of the functional and evolutionary diversity within the MAPEG family and also provides insights into the structure of the related MGST1. The structure is in good agreement with available biochemical data, in some cases offering alternative interpretations. Based on the structure, we also propose a mechanism for the catalytic activity and potential roles of the central cavity. However, additional studies will be required to verify these hypotheses. The structures presented here provide an excellent starting point for rational inhibitor design. Because the active site is shallow and located within the membrane-spanning region, computational methods will be complicated by the need for modeling of the membrane. Additional protein-ligand structures would be of great value for the development of therapeutics for inflammatory pain and cancer.

Materials and Methods

Protein Expression and Purification. The human mPGES-1 (GenBank accession no. BC008280) was PCR-cloned from a placenta cDNA library. The coding sequence of mPGES-1 was inserted into a baculovirus DNA using BaculoDirect baculovirus expression system (Invitrogen) according to the manufacturer's instructions. The recombinant virus was amplified and used to infect Sf9 cells cultivated in Sf-900 media (Invitrogen) with a multiplicity-of-titer of 2 at a cell density of 3×10^6 cells/mL. mPGES-1 was purified according to Ouellet et al. (28). Briefly, cells were harvested 70 h postinfection by centrifugation and resuspended in 15 mM Tris·HCl pH 8, 0.25 M Sucrose, 0.1 mM EDTA, and 1 mM reduced L-glutathione (GSH, Fluka). After disruption of the cells, a microsomal fraction was prepared by ultracentrifugation and the mPGES-1 was solubilized from the membranes by addition of 3% (wt/vol) β-octyl-glucoside (n-octyl β-D-glucopyranoside, Anatrace) in 10 mM potassium phosphate pH 7, 10% (wt/vol) glycerol, 0.1 mM EDTA, and 1 mM GSH. The solubilized enzyme was finally purified on hydroxylapatite (Macroprep ceramic hydroxylapatite type 1, BioRad). The experimental relative molecular mass was 16971, 131 less than the calculated mass based on sequence (17102), because of a lack of N-terminal methionine. Enzyme activity of mPGES-1 was studied biochemically by determining net enzymatic conversion of added PGH_2 (Larodan Fine Chemicals) in potassium phosphate buffer [50 mM pH 6.8, 2.5 mM GSH, and 1% (wt/vol) β-octyl glucoside] to PGE_2 by use of an HTRF kit (Cisbio International, 62PG2PEC). The purified mPGES-1 was found to be active.

Crystallization and Structure Determination. For crystallization, the protein buffer was exchanged to 10 mM Hepes pH 7.4, 1 mM GSH, and 1% β octyl-glucoside and the mPGES-1 sample was concentrated to 15 mg/mL. Crystals were grown in the presence of β-octyl-glycoside and GSH or 1-(4-phenyl-phenyl)-2-(S-glutathionyl)-ethanone [bis-phenyl-GSH; synthesized as described previously (29)] at 4 °C by the hanging drop vapor diffusion method by mixing the protein with an equal volume of reservoir solution. Reservoir solutions used contained 100 mM CAPSO pH 9.5, 30% PEG400, 100 mM NaCl, and 100 mM Li_2SO_4 (mersalyl acid soak and bis-phenyl-GSH complex) or 100 mM Tris pH 8.0–8.5, 30% PEG400, 100 mM NaCl, and 1 mM TCEP (native GSH complex).

The structure of mPGES-1 in complex with GSH was solved using the anomalous dispersion from mercury atoms incorporated into mPGES-1 crystals by soaking. The reaction was stopped after 6 h by flash freezing the crystal in liquid nitrogen. Native and derivative datasets were collected at beam line ID14 EH4 (Native1, Native 2, and mersalyl acid soaked crystals) and ID23 (bis-phenyl-GSH cocrystal) at the European Synchrotron Radiation Facility. The data were processed using MOSFLM (30), scaled and further reduced using the Collaborative Computational Project 4 suite of programs (31); for statistics, see Table S1. Despite the apparent isomorphism of the native and derivative datasets, it was not possible to merge them. Instead, phasing was done using single wavelength anomalous dispersion. The positions of two mercury sites were identified with the program SOLVE (32) using all data to 1.8 Å. The solution had a Z score of 5.7 and an overall mean figure of merit of 0.21. The resulting map was subjected to density modification using the program DM in the Collaborative Computational Project 4 suite (31). The resulting map was clearly interpretable and an initial model consisting of 138 residues (91% of the asymmetric unit content) was automatically built using ARP/wARP (33); the resulting figure of merit was 0.795. The model was used for molecular replacement with Molrep (31) of the 1.16 Å native dataset as well as the bis-phenyl-GSH complex. Model rebuilding was performed within Coot (34) and refinement was performed using REFMAC5 (31). The data allowed detailed modeling of dual conformation of side chains and solvent molecules. Although the data may allow for accurate modeling of occupancies of side chain conformations, we chose to set all nonunity occupancies to 0.5. Pictures were prepared using Pymol (35) unless otherwise stated. For statistics of the final model, see Table S1.

ACKNOWLEDGMENTS. We thank Stefan Schmidt, Thomas Falkman for large-scale cell culture, Pernilla Löfås and Mats Ormö for help with purification of mPGES-1, and Martin Johansson for the synthesis of 1-(4-phenyl-phenyl)-2-(S-glutathionyl)-ethanone. We are also grateful to the European Synchrotron Radiation Facility staff for assistance with data collection.

1. Funk CD (2001) Prostaglandins and leukotrienes: Advances in eicosanoid biology. *Science* 294(5548):1871–1875.
2. Samuelsson B, Morgenstern R, Jakobsson PJ (2007) Membrane prostaglandin E synthase-1: A novel therapeutic target. *Pharmacol Rev* 59(3):207–224.
3. Rådmark O, Samuelsson B (2010) Microsomal prostaglandin E synthase-1 and 5-lipoxygenase: Potential drug targets in cancer. *J Intern Med* 268(1):5–14.
4. Grosser T, Fries S, FitzGerald GA (2006) Biological basis for the cardiovascular consequences of COX-2 inhibition: Therapeutic challenges and opportunities. *J Clin Invest* 116(1):4–15.
5. Wu D, et al. (2009) Comparison of microsomal prostaglandin E synthase-1 deletion and COX-2 inhibition in acute cardiac ischemia in mice. *Prostaglandins Other Lipid Mediat* 90(1-2):21–25.
6. Jakobsson PJ, Morgenstern R, Mancini J, Ford-Hutchinson A, Persson B (1999) Common structural features of MAPEG—A widespread superfamily of membrane associated proteins with highly divergent functions in eicosanoid and glutathione metabolism. *Protein Sci* 8(3):689–692.
7. Bresell A, et al. (2005) Bioinformatic and enzymatic characterization of the MAPEG superfamily. *FEBS J* 272(7):1688–1703.
8. Hebert H, et al. (1997) The 3.0 A projection structure of microsomal glutathione transferase as determined by electron crystallography of p 21212 two-dimensional crystals. *J Mol Biol* 271(5):751–758.
9. Schmidt-Krey I, et al. (2004) Human leukotriene C(4) synthase at 4.5 A resolution in projection. *Structure* 12(11):2009–2014.
10. Ferguson AD, et al. (2007) Crystal structure of inhibitor-bound human 5-lipoxygenase-activating protein. *Science* 317(5837):510–512.
11. Ago H, et al. (2007) Crystal structure of a human membrane protein involved in cysteinyl leukotriene biosynthesis. *Nature* 448(7153):609–612.
12. Martinez Molina D, et al. (2007) Structural basis for synthesis of inflammatory mediators by human leukotriene C4 synthase. *Nature* 448(7153):613–616.
13. Holm PJ, et al. (2006) Structural basis for detoxification and oxidative stress protection in membranes. *J Mol Biol* 360(5):934–945.
14. Jegerschöld C, et al. (2008) Structural basis for induced formation of the inflammatory mediator prostaglandin E2. *Proc Natl Acad Sci USA* 105(32):11110–11115.
15. Martinez Molina D, Eshaghi S, Nordlund P (2008) Catalysis within the lipid bilayer-structure and mechanism of the MAPEG family of integral membrane proteins. *Curr Opin Struct Biol* 18(4):442–449.
16. He S, Wu Y, Yu D, Lai L (2011) Microsomal prostaglandin E synthase-1 exhibits one-third-of-the-sites reactivity. *Biochem J* 440(1):13–21.
17. Alander J, et al. (2009) Microsomal glutathione transferase 1 exhibits one-third-of-the-sites-reactivity towards glutathione. *Arch Biochem Biophys* 487(1):42–48.
18. Rinaldo-Matthis A, et al. (2010) Arginine 104 is a key catalytic residue in leukotriene C4 synthase. *J Biol Chem* 285(52):40771–40776.
19. Hammarberg T, et al. (2009) Mutation of a critical arginine in microsomal prostaglandin E synthase-1 shifts the isomerase activity to a reductase activity that converts prostaglandin H2 into prostaglandin F2alpha. *J Biol Chem* 284(1):301–305.
20. Ji X, et al. (1994) Structure and function of the xenobiotic substrate binding site of a glutathione S-transferase as revealed by X-ray crystallographic analysis of product complexes with the diastereomers of 9-(S-glutathionyl)-10-hydroxy-9,10-dihydrophenanthrene. *Biochemistry* 33(5):1043–1052.
21. Li Y, Angelastro M, Shimshock S, Reiling S, Vaz RJ (2010) On the mechanism of microsomal prostaglandin E synthase type-2—A theoretical study of endoperoxide reaction with MeS(-). *Bioorg Med Chem Lett* 20(1):338–340.
22. Guillén Schlippe YV, Hedstrom L (2005) A twisted base? The role of arginine in enzyme-catalyzed proton abstractions. *Arch Biochem Biophys* 433(1):266–278.
23. Kobilka BK, Deupi X (2007) Conformational complexity of G-protein-coupled receptors. *Trends Pharmacol Sci* 28(8):397–406.
24. Dahl SG, Sylte I, Ravna AW (2004) Structures and models of transporter proteins. *J Pharmacol Exp Ther* 309(3):853–860.
25. Prage EB, et al. (2011) Location of inhibitor binding sites in the human inducible prostaglandin E synthase, MPGES1. *Biochemistry* 50(35):7684–7693.
26. Xu D, et al. (2008) MF63 [2-(6-chloro-1H-phenanthro[9,10-d]imidazol-2-yl)-isophthalonitrile], a selective microsomal prostaglandin E synthase-1 inhibitor, relieves pyresis and pain in preclinical models of inflammation. *J Pharmacol Exp Ther* 326(3):754–763.
27. Pawelzik SC, et al. (2010) Identification of key residues determining species differences in inhibitor binding of microsomal prostaglandin E synthase-1. *J Biol Chem* 285(38):29254–29261.
28. Ouellet M, et al. (2002) Purification and characterization of recombinant microsomal prostaglandin E synthase-1. *Protein Expr Purif* 26(3):489–495.
29. Shin SS, Lim D, Lee K (2003) Designing of non-hydrolyzing derivatives for GlxII inhibitors: Importance of hydrophobic moiety in S-site. *Bull Korean Chem Soc* 24: 897–898.
30. Leslie AG (1999) Integration of macromolecular diffraction data. *Acta Crystallogr D Biol Crystallogr* 55(Pt 10):1696–1702.
31. Collaborative Computational Project (1994) The CCP4 suite: Programs for protein crystallography. *Acta Crystallogr D Biol Crystallogr* 50:750–763.
32. Terwilliger TC, Berendzen J (1999) Automated MAD and MIR structure solution. *Acta Crystallogr D Biol Crystallogr* 55(Pt 4):849–861.
33. Perrakis A, Morris R, Lamzin VS (1999) Automated protein model building combined with iterative structure refinement. *Nat Struct Biol* 6(5):458–463.
34. Emsley P, Cowtan K (2004) Coot: Model-building tools for molecular graphics. *Acta Crystallogr D Biol Crystallogr* 60(Pt 12 Pt 1):2126–2132.
35. DeLano WL (2001) *The PyMOL Molecular Graphics System* (DeLano Scientific, Palo Alto, CA).